J|A|C|S ARTICLES

Published on Web 07/29/2009

Relaxation Dynamics of *Pseudomonas aeruginosa* $Re^{I}(CO)_3(\alpha\text{-diimine})(HisX)^{+}$ (X = 83, 107, 109, 124, 126)Cu^{II} Azurins

Ana María Blanco-Rodríguez,[†] Michael Busby,[†] Kate Ronayne,[‡] Michael Towrie,[‡] Cristian Grădinaru,[§] Jawahar Sudhamsu,[§] Jan Sýkora,[||] Martin Hof,[||] Stanislav Záliš,[||] Angel J. Di Bilio,[⊥] Brian R. Crane,*[,§] Harry B. Gray,*[,⊥] and Antonín Vlček, Jr.*[,†,||]

School of Biological and Chemical Sciences, Queen Mary, University of London, Mile End Road, London E1 4NS, United Kingdom, Central Laser Facility, CCLRC Rutherford Appleton Laboratory, Chilton, Didcot, Oxfordshire OX11 0QX, United Kingdom, Department of Chemistry and Chemical Biology, Cornell University, Ithaca, New York 14853, J. Heyrovský Institute of Physical Chemistry, Academy of Sciences of the Czech Republic, Dolejškova 3, 182 23 Prague, Czech Republic, and Beckman Institute, California Institute of Technology, Pasadena, California 91125

Received April 10, 2009; E-mail: a.vlcek@qmul.ac.uk; bc69@cornell.edu; hbgray@caltech.edu

Abstract: Photoinduced relaxation processes of five structurally characterized *Pseudomonas aeruginosa* $Re^{I}(CO)_3(\alpha\text{-diimine})(HisX)$ (X = 83, 107, 109, 124, 126)Cu^{II} azurins have been investigated by time-resolved (ps−ns) IR spectroscopy and emission spectroscopy. Crystal structures reveal the presence of Re-azurin dimers and trimers that in two cases (X = 107, 124) involve van der Waals interactions between interdigitated diimine aromatic rings. Time-dependent emission anisotropy measurements confirm that the proteins aggregate in mM solutions (D_2O, KP_i buffer, pD = 7.1). Excited-state DFT calculations show that extensive charge redistribution in the $Re^{I}(CO)_3 \rightarrow$ diimine ^{3}MLCT state occurs: excitation of this ^{3}MLCT state triggers several relaxation processes in Re-azurins whose kinetics strongly depend on the location of the metallolabel on the protein surface. Relaxation is manifested by dynamic blue shifts of excited-state ν(CO) IR bands that occur with triexponential kinetics: intramolecular vibrational redistribution together with vibrational and solvent relaxation give rise to subps, ∼2, and 8−20 ps components, while the $\sim 10^2$ ps kinetics are attributed to displacement (reorientation) of the $Re^{I}(CO)_3$(phen)(im) unit relative to the peptide chain, which optimizes Coulombic interactions of the Re^{I} excited-state electron density with solvated peptide groups. Evidence also suggests that additional segmental movements of Re-bearing β-strands occur without perturbing the reaction field or interactions with the peptide. Our work demonstrates that time-resolved IR spectroscopy and emission anisotropy of Re^{I} carbonyl−diimine complexes are powerful probes of molecular dynamics at or around the surfaces of proteins and protein−protein interfacial regions.

Introduction

Long-range electron transfer (ET) reactions in proteins and other complex media often are strongly modulated by donor−bridge−acceptor dynamics. A case in point is cytochrome b_{562}, where picosecond peptide-chain structural fluctuations determine whether the heme electronic coupling to a distant surface-attached Ru(III) involves a single specific superexchange pathway or a multitude of interacting pathways.[1] ET driving forces, reorganization energies, and donor−acceptor distances are all influenced by relaxation dynamics.[2−4] Of special importance in this context are the interfacial fluctuations associated with protein−protein ET reactions,[5−7] which, like peptide conformational dynamics or solvent reorganization, can be rate limiting.[8] Induced dynamics can affect ultrarapid (fs−ns) excited-state ET, since electronic excitation of the donor or acceptor triggers comparably fast movements in its vicinity, caused by dissipation of vibrational energy and a virtually instantaneous change in charge distribution.

Labeling protein surfaces with $Re^{I}(CO)_3(N,N)$(imidazole)[9−11] (N,N = α-diimine) opens the way for investigations of relaxation dynamics in the region around one of the redox centers under the same conditions that normally trigger ET. Owing to the high sensitivity of CO stretching vibrations to structural perturbations

[†] University of London.
[‡] CCLRC Rutherford Appleton Laboratory.
[§] Cornell University.
[||] Academy of Sciences of the Czech Republic.
[⊥] California Institute of Technology.

(1) Prytkova, T. R.; Kurnikov, I. V.; Beratan, D. N. *Science* **2007**, *315*, 622–625.
(2) Skourtis, S. S.; Balabin, I. A.; Kawatsu, T.; Beratan, D. N. *Proc. Natl. Acad. Sci. U.S.A.* **2005**, *102*, 3552–3557.
(3) Balabin, I.; Onuchic, J. N. *Science* **2000**, *290*, 114–117.
(4) Gray, H. B.; Winkler, J. R. *Proc. Natl. Acad. Sci. U.S.A.* **2005**, *102*, 3534–3539.
(5) Hoffman, B. M.; Celis, L. M.; Cull, D. A.; Patel, A. D.; Seifert, J. L.; Wheeler, K. E.; Wang, J.; Yao, J.; Kurnikov, I. V.; Nocek, J. M. *Proc. Natl. Acad. Sci. U.S.A.* **2005**, *102*, 3564–3569.
(6) Wheeler, K. E.; Nocek, J. M.; Cull, D. A.; Yatsunyk, L. A.; Rosenzweig, A. C.; Hoffman, B. M. *J. Am. Chem. Soc.* **2007**, *129*, 3906–3917.
(7) Miyashita, O.; Okamura, M. Y.; Onuchic, J. N. *Proc. Natl. Acad. Sci. U.S.A.* **2005**, *102*, 3558–3563.
(8) Bixon, M.; Jortner, J. *Adv. Chem. Phys.* **1999**, *106*, 35–202.

 10.1021/ja902744s CCC: $40.75

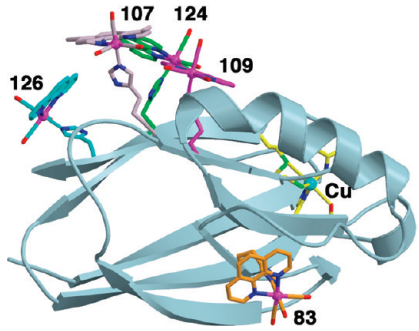

Figure 1. *Pseudomonas aeruginosa* azurins labeled with Re^{I}(CO)$_3$(N,N)(HisX) at five surface positions (*N*,*N* = 1,10-phenanthroline (phen) for X = 83, 109, 124, 126; N,N = 4,7-dimethyl-1,10-phen (dmp) for X = 107, 124).

and changes in electron-density distributions, it is possible to follow relaxation of an electronically excited Re^{I} label using time-resolved IR (TRIR) spectroscopy.[12−18]

Pseudomonas aeruginosa azurins are ideal systems for investigations of protein dynamics associated with long-range ET reactions.[2] They provide a structurally well characterized scaffold where metal-containing sensitizers can be attached at defined positions, allowing for definitive investigations[4,10,11,19−23] of electron tunneling through a folded polypeptide. Importantly, multistep tunneling through an intervening tryptophan in the protein dramatically accelerates ET from Cu^{I} to an electronically excited Re^{I} carbonyl-diimine 20 Å away.[24] In the course of these investigations, we have discovered that electronic excitation of Re(CO)$_3$(phen)(im) at Re-azurin surface sites (Figure 1) also triggers relaxation processes and structural dynamics on time scales comparable with those of picosecond to early nanosecond ET reactions.

Experimental Section

fac-[Re(im)(CO)$_3$(phen)]$_2$SO$_4$·4H$_2$O, **Re(im)**, and Re-modified azurins were prepared as described previously.[9−11] The Cu^{II} Re-azurins were equilibrated with D$_2$O by repeatedly concentrating/diluting with deuterated buffer using Centricon devices. All solutions for TRIR spectra were prepared in air-saturated D$_2$O containing 0.0268 m Na$_2$HPO$_4$ and 0.0196 m KH$_2$PO$_4$ to give a pD ≅ 7 buffer.

Crystals of [Re^{I}(CO)$_3$(phen)(Thr124His)]$^{+}$-(His83Gln)AzCu(II), **124-phen** (space group *P*1, cell dimensions 30.13 × 58.98 × 66.11 Å^3; α = 82.92°, β = 78.11°, γ = 76.68°, four molecules per asymmetric unit), grew from 2.5 μL drops made from 1 μL of 30 mg/mL Re^{I}-azurin in 25 mM HEPES pH 7.5, 0.5 μL of saturated [Co(NH$_3$)$_5$Cl]Cl$_2$, and 1 μL reservoir. The drops were equilibrated against 500 μL of reservoir containing 20% PEG molecular weight 4000, 100 mM LiNO$_3$, and 100 mM imidazole pH 7.0. Diffraction data (30.0−1.35 Å resolution, 95.6% complete, $R_{sym} = \sum_j |I_j - \langle I \rangle| / \sum\sum_j I_j$ = 8.8%; overall signal-to-noise = $\langle I \rangle / \sigma I$ = 4.7) were collected on a Quantum-210 CCD (Area Detector Systems Corporation) at the Cornell High Energy Synchrotron Source, beamline F2 (0.916 Å) and processed with DENZO.[25] The structure of **124-phen** was determined by molecular replacement with EPMR[26] using a probe derived from the structure of Ru-labeled azurin (PDB code: 1BEX).[27] Rigid-body, positional, and thermal factor refinement with CNS,[28] amidst rounds of manual rebuilding, Re^{I}(CO)$_3$(phen) incorporation, and water placement with XFIT,[29] followed by further anisotropic refinement of all heavy atoms' temperature factors (S, Cu, and Re) with SHELX-97[30] produced the final model (1.35 Å resolution, *R*-factor = 20.5%; *R*-free = 23.9%). The refinement was performed against all but 5% of the reflections, which were used to calculate an *R*-free value. The final round of refinement was performed against the entire data set. All residues have favored backbone dihedral angles. Stereochemical restraints were removed from the copper ligand bonds in the later stages of refinement. Coordinates and additional data collection/refinement statistics are deposited in the Protein Data Bank as PDB code 2i7s.

Crystals of [Re^{I}(CO)$_3$(phen)(Thr126His)]$^{+}$-(His83Gln)AzCu(II), **126-phen** (space group $P2_1$, 44.48 × 56.71 × 97.82 Å^3, α = 90.0°, β = 102.70°, γ = 90.0°), were grown under the same conditions as those for **124-phen** except that [Co(NH$_3$)$_5$Cl]Cl$_2$ was not used. Diffraction data (resolution 30.0−1.45 Å; R_{sym} 0.087, 99.8% complete, $\langle I \rangle / \sigma I$ = 5.1) were collected at the CHESS synchrotron beamline F1 (0.9480 Å) and processed with Mosflm. Molecular replacement with the **124-phen** structure as probe placed four molecules in the asymmetric unit. Model building and refinement followed the same procedure given above to give a final model with *R*-factor = 20.6%, *R*-free = 21.6% to 1.45 Å resolution (PDB code: 3IBO).

The structure of the [Re^{I}(CO)$_3$(dmp)(Gln107His)]$^{+}$-(His83Gln)-AzCu(II) has been determined (PDB code: 1i53).[10,22] Photophysical experiments were performed on a mutant (abbreviated **107-dmp)** where Tyr108, Tyr72, and Trp48 were replaced by phenylalanine.

(9) Connick, W. B.; Di Bilio, A. J.; Hill, M. G.; Winkler, J. R.; Gray, H. B. *Inorg. Chim. Acta* **1995**, *240*, 169–173.
(10) Di Bilio, A. J.; Crane, B. R.; Wehbi, W. A.; Kiser, C. N.; Abu-Omar, M. M.; Carlos, R. M.; Richards, J. H.; Winkler, J. R.; Gray, H. B. *J. Am. Chem. Soc.* **2001**, *123*, 3181–3182.
(11) Crane, B. R.; Di Bilio, A. J.; Winkler, J. R.; Gray, H. B. *J. Am. Chem. Soc.* **2001**, *123*, 11623–11631.
(12) Liard, D. J.; Busby, M.; Matousek, P.; Towrie, M.; Vlček, A., Jr. *J. Phys. Chem. A* **2004**, *108*, 2363–2369.
(13) Blanco-Rodríguez, A. M.; Ronayne, K. L.; Záliš, S.; Sýkora, J.; Hof, M.; Vlček, A., Jr. *J. Phys. Chem. A* **2008**, *112*, 3506–3514.
(14) Blanco-Rodríguez, A. M.; Towrie, M.; Collin, J.-P.; Záliš, S.; Vlček, A., Jr. *Dalton Trans.* **2009**, 3941–3949.
(15) Asbury, J. B.; Wang, Y.; Lian, T. *Bull. Chem. Soc. Jpn.* **2002**, *75*, 973–983.
(16) Lenchenkov, V. A.; She, C.; Lian, T. *J. Phys. Chem. B* **2004**, *108*, 16194–16200.
(17) Bredenbeck, J.; Helbing, J.; Hamm, P. *Phys. Rev. Lett.* **2005**, *95*, 083201.
(18) Blanco-Rodríguez, A. M.; Busby, M.; Grădinaru, C.; Crane, B. R.; Di Bilio, A. J.; Matousek, P.; Towrie, M.; Leigh, B. S.; Richards, J. H.; Vlček, A., Jr.; Gray, H. B. *J. Am. Chem. Soc.* **2006**, *128*, 4365–4370.
(19) Miller, J. E.; Di Bilio, A. J.; Wehbi, W. A.; Green, M. T.; Museth, A. K.; Richards, J. R.; Winkler, J. R.; Gray, H. B. *Biochim. Biophys. Acta* **2004**, *1655*, 59–63.
(20) Winkler, J. R.; Di Bilio, A. J.; Farrow, N. A.; Richards, J. H.; Gray, H. B. *Pure Appl. Chem.* **1999**, *71*, 1753–1764.
(21) Tezcan, F. A.; Crane, B. R.; Winkler, J. R.; Gray, H. B. *Proc. Natl. Acad. Sci. U.S.A.* **2001**, *98*, 5002–5006.
(22) Miller, J. E.; Gradinaru, C.; Crane, B. R.; Di Bilio, A. J.; Wehbi, W. A.; Un, S.; Winkler, J. R.; Gray, H. B. *J. Am. Chem. Soc.* **2003**, *125*, 14220–14221.
(23) Regan, J. J.; Onuchic, J. N. *Adv. Chem. Phys.* **1999**, *107*, 497–554.
(24) Shih, C.; Museth, A. K.; Abrahamsson, M.; Blanco-Rodriguez, A. M.; Di Bilio, A. J.; Sudhamsu, J.; Crane, B. R.; Ronayne, K. L.; Towrie, M.; Vlček, A., Jr.; Richards, J. H.; Winkler, J. R.; Gray, H. B. *Science* **2008**, *320*, 1760–1762.
(25) Otwinowski, Z.; Minor, W. In *Methods in Enzymology, Volume 276, Macromolecular Crystallography, Part A*; Carter, C. W., Jr., Sweet, R. M., Eds.; Academic Press: 1997, pp 307−326.
(26) Kissinger, C. R.; Gehlhaar, D. K.; Fogel, D. B. *Acta Crystallogr.* **1999**, *D55*, 484–491.
(27) Faham, S.; Day, M. W.; Connick, W. B.; Crane, B. R.; Di Bilio, A. J.; Schaefer, W. P.; Rees, D. C.; Gray, H. B. *Acta Crystallogr.* **1999**, *D55*, 379–385.
(28) Brunger, A.; Adams, P. D.; Clore, G. M.; DeLano, W. L.; Gros, P.; Grosse-Kunstleve, R. W.; Jiang, J. S.; Kuszewski, J.; Nilges, M.; Pannu, N. S.; Read, R. J.; Rice, L. M.; Simonson, T.; Warren, G. L. *Acta Crystallogr.* **1998**, *D54* (Part 5 SEP 1), 905–921.
(29) McRee, D. E. *J. Mol. Graphics* **1992**, *10*, 44–46.
(30) Sheldrick, G. M.; Schneider, T. R. *Macromol. Crystallogr., Part B* **1997**, *277*, 319–343.

A high-resolution structure of this "all-Phe" mutant (unpublished results) shows that the Re binding sites in the two Re-His107 azurins are virtually identical. X-ray structures of **83-phen**[11,18] and **109-phen**[18] also have been reported. The respective PDB codes are 1JZI and 2FNW.

UV−vis and FTIR absorption spectra were recorded using HP8453 and PE1720X spectrometers, respectively. Emission spectra were obtained on Jobin Yvon (Horiba) FluoroMax-3 and Fluorolog-3 instruments.

Time-resolved IR measurements and procedures have been described in detail.[31,32] In short, the sample solution was excited (pumped) at 400 nm, using frequency-doubled pulses from a Ti: sapphire laser of ~150 fs duration (fwhm) and *ca.* 3 μJ of energy, focused at an area ~200 μm in diameter. TRIR spectra were probed with IR (~150 fs) pulses obtained by difference-frequency generation. The IR probe pulses cover a 150−200 cm^{-1} spectral range. The sample solutions were placed in a *ca.* 0.05 mm deep round dip drilled into a CaF_2 plate and tightly covered with a polished CaF_2 window. The cell was scanned-rastered across the area of the dip in two dimensions to prevent laser heating and decomposition of the sample. FTIR spectra measured before and after the experiment demonstrated sample stability. Bands observed in TRIR spectra were fitted by a sum of Lorentzian or Gaussian functions to determine accurately their center positions and shapes. Although entire spectra can be fitted in this way, most of the data were obtained from fits that included the middle A′(2) excited-state band, the A′(1) bleach, and the A′(1) excited-state band. These fits allowed us to determine rather accurately the position of the A′(1) excited-state band. The same fitting procedure was used for all spectra measured, ensuring good relative comparability of results obtained for the different species. All spectral and kinetics fitting procedures were performed using MicroCal Origin 7.0.

Emission lifetime and time-resolved anisotropy measurements were performed using time-correlated single-photon counting (TCSPC) on an IBH 5000 U instrument equipped with a cooled Hamamatsu R3809U-50 microchannel plate photomultiplier. The **Re(im)**, **83-phen**, **107-dmp**, **109-phen**, and **124-phen** samples were excited at 405 nm and **126-phen** was excited at 370 nm with diode lasers IBH NanoLED-07 (fwhm 80 ps, 500 kHz repetition rate, IBH) or NanoLED-03 (fwhm 100 ps, 500 kHz repetition rate), respectively. The emission monochromator was set to a wavelength corresponding to the emission maximum. Data were analyzed using IBH Datastation2 software. Values of the anisotropy were calculated as follows:

$$r(t) = \frac{I_{vv}(t) - GI_{vh}(t)}{I_{vv}(t) + 2GI_{vh}(t)} \quad (1)$$

where I_{vv} and I_{vh} are the intensities recorded at different orientations of the polarizers; i.e., "*v*" and "*h*" subscripts represent the vertical and horizontal directions, respectively. The first and second subscripts denote the direction plane of the polarization in the excitation and emission arm, respectively, and G is the correction factor. The calculated anisotropy decays were then fitted with a biexponential decay:

$$r(t) = a_1 \exp(-t/T_1) + a_2 \exp(-t/T_2) \quad (2)$$

where T_1 and T_2 are the fast and slow rotation correlation times, respectively, and the a_i values are the corresponding amplitudes. The initial anisotropy $r(0)$ is defined as $a_1 + a_2$. Separate anisotropy measurements were performed in two time ranges, 0−215 ns (resolution of 228 ps/channel) and 0−9.2 ns (11.6 ps/channel), to capture slow and the fast anisotropy decays, respectively. The slow rotation time was determined first from the long-range measurement, and its value was fixed when fitting the short-range anisotropy decay curves. The sample temperature was kept at 21 °C.

The electronic structure of $[Re(CO)_3(phen)(Etim)]^+$, **Re(Etim)**, was calculated by density functional theory (DFT) methods using the Gaussian 03[33] program package, employing the hybrid functional PBE0.[34,35] Electronic transitions were calculated by the time-dependent DFT (TDDFT) method. The structure of the lowest triplet excited state a^3A was optimized by UKS calculations. For H, C, N, O atoms, 6-311g* polarized triple-ζ basis sets[36] were used for geometry optimization and vibrational analysis, while cc-pvdz correlation consistent polarized valence double-ζ basis sets[37] were employed in TDDFT, total density, and electrostatic potential calculations. Quasirelativistic effective core pseudopotentials and a corresponding optimized set of basis functions for Re were employed.[38] The solvent was described by a polarizable conductor calculation model (CPCM).[39] The electron density differences and electrostatic potential plots were drawn using the GaussView program. Energies and compositions of frontier Kohn−Sham MOs are summarized in Tables S2, S3. Lowest singlet electronic transitions are listed in Tables S4, S5. Optimized ground- and lowest excited-state conformations are shown in Figures S1−2 and S3−4, respectively.

Results

Re Binding Site Structures and FTIR Spectra. X-ray structures of the Re binding sites in the five azurins are shown in Figure 2. Both **107-dmp** and **124-phen** make strong intermolecular contacts in crystals due to $\pi\pi$ stacking and interdigitation of phen ligands on opposing molecules. In **124-phen**, the phen ligands "hook" each other across a symmetric interface and generate a dimer of azurin molecules. In **107-dmp**, two dmp ligands interact in a similar fashion; however, a closed dimer is not formed and the interface rather involves three azurin molecules within the crystal lattice. Both $Re(CO)_3$(phen) units of **124-phen** lie at the surface of the azurin dimer and are relatively exposed to the surrounding medium. Both of them have similar environments in which the axial and the two equatorial CO ligands interact only with water molecules; one equatorial CO is directed at Lys122 and Gln107 but is not close enough to hydrogen bond to these residues. (The closest interaction is to the side chain of Lys122, 4−5 Å apart depending on the molecule in the asymmetric unit.) In both molecules the distal side of the phen ring is solvated. In contrast, the Re binding site in **107-dmp** is much more sequestered than in **124-phen**. The dmp ligands of both $Re(CO)_3$(dmp) units of **107-dmp** lie in the groove between the two other azurins in the lattice. In one molecule the distal side of the dmp ligand stacks against the Ala53-Ala54 peptide bond of a neighboring molecule, whereas in the other the dmp ligand makes contacts with Thr124 and Met109. The environment of the CO ligands is rather different in the two molecules that make up the interface. The axial CO of the first molecule inserts into a tight

(31) Towrie, M.; Grills, D. C.; Dyer, J.; Weinstein, J. A.; Matousek, P.; Barton, R.; Bailey, P. D.; Subramaniam, N.; Kwok, W. M.; Ma, C. S.; Phillips, D.; Parker, A. W.; George, M. W. *Appl. Spectrosc.* **2003**, *57*, 367–380.
(32) Vlček, A., Jr.; Farrell, I. R.; Liard, D. J.; Matousek, P.; Towrie, M.; Parker, A. W.; Grills, D. C.; George, M. W. *J. Chem. Soc., Dalton Trans.* **2002**, 701–712.
(33) Frisch, M. J.; et al. *Gaussian 03*; Gaussian, Inc.: Wallingford, CT, 2004.
(34) Perdew, J. P.; Burke, K.; Ernzerhof, M. *Phys. Rev. Lett.* **1996**, *77*, 3865.
(35) Adamo, C.; Barone, V. *J. Chem. Phys.* **1999**, *110*, 6158–6170.
(36) Krishnan, R.; Binkley, J. S.; Seeger, R.; Pople, J. A. *J. Chem. Phys.* **1980**, *72*, 650–654.
(37) Woon, D. E.; Dunning, T. H., Jr. *J. Chem. Phys.* **1993**, *98*, 1358.
(38) Andrae, D.; Häussermann, U.; Dolg, M.; Stoll, H.; Preuss, H. *Theor. Chim. Acta* **1990**, *77*, 123–141.
(39) Cossi, M.; Rega, N.; Scalmani, G.; Barone, V. *J. Comput. Chem.* **2003**, *24*, 669.

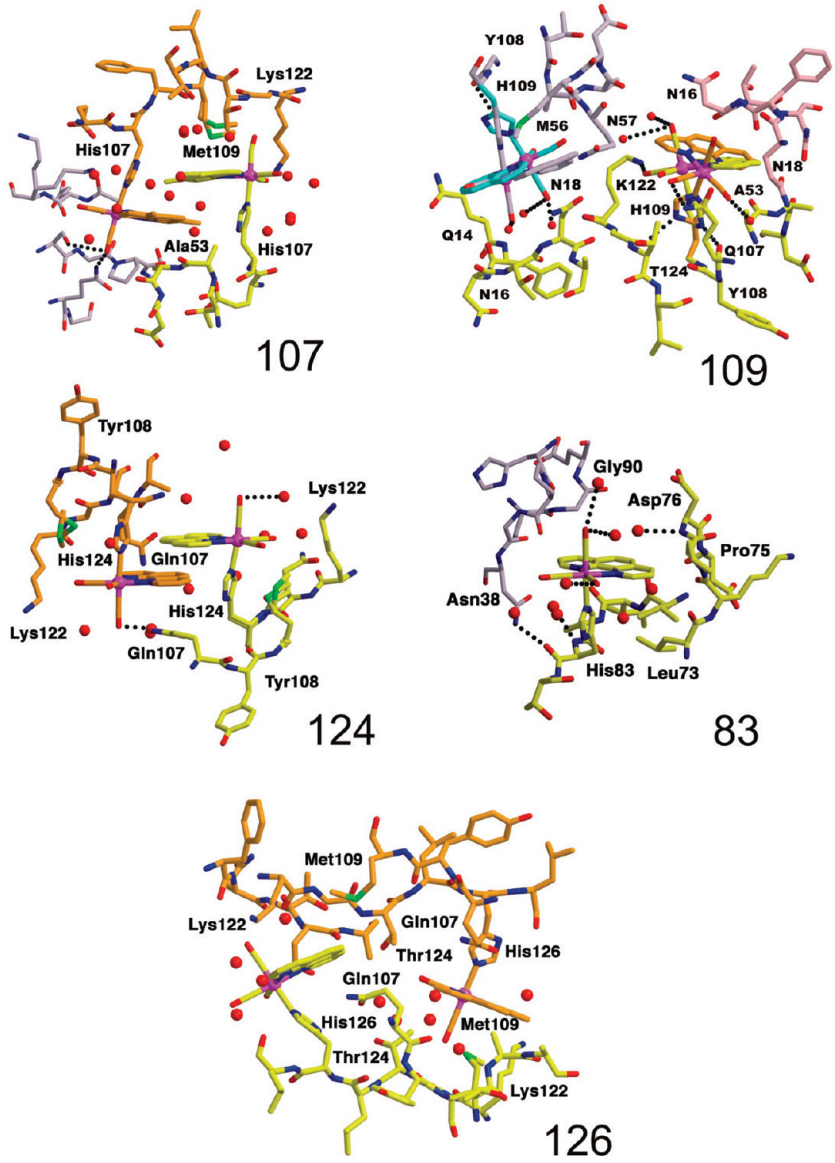

Figure 2. Structures of the metallolabel region of Re^{I}(CO)$_3$(phen)(HisX) and Re^{I}(CO)$_3$(dmp)(His107) azurins. Individual species are denoted by the His ligand X: **83-phen**, **107-dmp**, **109-phen**, **124-phen**, **126-phen**. The model complex [Re^{I}(CO)$_3$(phen)(im)]$^+$ is abbreviated **Re(im)**.

pocket formed by Pro36 and hydrogen bonds to Gln8 and Ser34. The other axial CO lies between the side chains of Met109 and Lys122, each on adjacent β-strands. The equatorial COs of both molecules are partially solvated, but again in quite different environments. In one molecule there is a long H-bond to the Lys122 side chain from a neighboring azurin molecule, as well as contacts with the surrounding solvent. Notably, another **107-dmp** variant, which has Tyr108 replaced with Trp, crystallizes in a different space group but shows the same Re-mediated association mode involving three azurin molecules (PDB code: 1r1c).[22] The structures of **83-phen**[11,18] and **109-phen**[18] show that these two azurins are not associated by "hooked" Re dimers. Two conformers are seen for **109-phen**, which differ in the orientation of Re(CO)$_3$(phen)(im) relative to the peptide. In both conformers, the carbonyl groups point away from the azurin surface. Hydrogen bonds between CO ligands and water molecules were detected in both species. Equatorial CO ligands in **109-phen** are involved in H-bonding with some of the peptide chain O- and N-atoms in the same azurin molecule. The flat faces of the phen ligand in **83-phen** and **109-phen** juxtapose the protein on one side and the solvent on the other.

The **126-phen** structure also forms a pseudosymmetric dimer in the crystal lattice, but the Re complexes do not directly interact because the Gln107 side chain on the same molecule inserts beneath the phen ligand, thereby preventing interdigitation of a phen from another protein. Gln107 and Thr124 lie roughly on the dimer axis and separate the two canted Re complexes. The dimer, however, is not perfectly symmetric. The distal face of each phen packs with Lys122 and Met109 of adjacent molecules, but in one case Lys122 dominates the contact, whereas in the other Met109 does. The phen contacts Gln107 of one protein and Met109 from the other. The Re complex binds against the C-terminal β-strand of the adjacent molecule but also against a β-turn protrusion involving residues 119−121 that leads into the C-terminal β-strand. The three carbonyls point toward the solvent and are all partially solvated. One of the equatorial carbonyls is within 4.0 Å of the C-terminal carboxylate of the same protein molecule. In the dimer, the axial CO projects against the other molecule.

Structures of the five Re-azurins indicate considerable rotational freedom around the Re−N(im) bond, whereby the orientation of the im(His) ligand relative to the Re(CO)$_2$(phen)

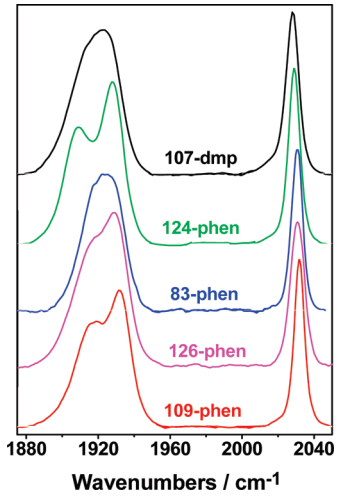

Figure 3. Ground-state FTIR spectra of the five Re-azurins in KP_i (D_2O, pD ~7.1) buffer.

Table 1. Ground- and Excited-State ν(CO) Energies of Re-Azurins and **Re(im)** Measured in KP_i (D_2O, pD ~7.1) Buffer[a]

	ground state			excited state (extrapolated to $t = \infty$)			$\Delta\nu$	$\Delta\nu$	$\Delta\nu$
	A′(2)	A″	A′(1)	A″	A′(2)	A′(1)	A″	A′(2)	A′(1)
Re(im)	1925	1925	2032	1967	2011	2070	42	86	38
107-dmp	1920	1920	2028	1961	2005	2052	41	85	24
83-phen	1923	1923	2031	1966	2010	2068	43	87	37
109-phen	1918	1932	2032	1961	2011	2068	29	93	36
124-phen	1909	1928	2029	1960	2009	2068	32	100	39
126-phen	1918	1929	2031	1962	2010	2066	33	92	35

[a] A″ and A′(2) excited-state wavenumbers are measured at long time delays (1 ns); A′(1) wavenumbers are extrapolated to infinite time delay ($\nu(\infty)$). Band assignments are based on work reported previously.[41−43]

symmetry plane ranges from nearly perpendicular (**109**) to parallel (**83**). The angles are given in Table S1. Accordingly, the DFT calculation of ground-state Re(Etim) in a vacuum (Figure S1) found two minima 0.027 eV apart. The only conformation calculated in H_2O is shown in Figure S2. It is apparent that the actual orientation is determined by constraints imposed by the peptide.

Ground-state FTIR spectra (Figure 3) of D_2O solutions of the Re-azurins in the spectral region of CO stretching vibrations, ν(CO), are typical of *fac*-tricarbonyls showing a relatively sharp band between 2028 and 2032 cm^{-1} attributable to the A′(1) in-phase symmetric vibration and a broad feature at lower energies that corresponds to the A′(2) out-of-phase symmetric stretch and the asymmetric equatorial A″ stretch (Table 1). (Labels refer to C_s local symmetry.) The A′(2) and A″ bands coalesce into a single band for **83-phen** and **107-dmp** (broad) and **Re(im)**, as is typical for *fac*-Re tricarbonyl complexes with three nitrogen-donor ligands. A distinct splitting between the A′(2) and A″ vibrations of 14 and 19 cm^{-1} is seen for **109-phen** and **124-phen**, respectively, while **126-phen** shows a shoulder. The A′(2)−A″ splitting appears when the equatorial and axial C≡O stretching force constants differ[40] or the two equatorial CO ligands are nonequivalent, as is the case for **109-phen** and **124-phen**, respectively.

Emission Spectra and Lifetimes. Each of the Re-azurins shows a broad phosphorescence (**107-dmp**: 553 nm; **124-phen**: 565 nm; **109-phen**: 557 nm; **83-phen**: 574 nm; **126-phen**: 578 nm) that occurs at slightly shorter wavelengths than that of **Re(im)**[9] or **Re(his)**,[44] 582 nm. The Re-azurin emission bands shift slightly to the red upon dilution, presumably because of a diminishing inner filter effect of the overlapping Cu^{II} absorption at *ca.* 630 nm. The emission decay kinetics are biexponential (Table 2): emission lifetimes of **83-phen** are independent of concentration; lifetimes of **109-phen**, **124-phen**, and **126-phen** show some changes upon the first dilution; decreasing the concentration of **107-dmp** is accompanied by a systematic decrease of the shorter lifetime τ_1 and increase of the longer lifetime τ_2; and a gradual decrease of τ_1 upon dilution also was observed for **126-phen**. The relative amplitude of the slow decay component increases upon dilution of all Re-azurins except **83-phen** and **126-phen** (this effect is most notable upon the first dilution of **109-phen**). The emission lifetimes are shortened relative to free **Re(im)** (120 ns),[9,10] **Re(im)(dmp)** (360 ns),[10] or **Re(his)** (100 ns)[44] (lifetimes in H_2O under argon) due to energy transfer to low-lying LF and LMCT states of Cu^{II}. The two decay kinetics components and their concentration dependences suggest that azurin aggregates of varying sizes and Re−Cu distances are present in solutions.

Time-Resolved Emission Anisotropy. Emission anisotropy of Re-azurins decays biexponentially on the background of a slower population decay. The photon count in the relevant time region is therefore rather low, increasing the data scatter (Figure 4), which in turn affects the absolute values of anisotropy decay lifetimes. The values reported in Table 3 were obtained using identical experimental and fitting procedures, as described in the Experimental Section and Figure 4. Thus, although the absolute T_1 and T_2 values should be regarded as estimates of the rotation lifetimes, their dependences on the azurin type and concentration have been determined with satisfactory accuracy. Experimental anisotropy decay curves are best fitted with a biexponential function (eq 2). Examination of **107-dmp** and **83-phen** anisotropy decays indicates that there may be a third decay component, but triexponential fitting leads to unrealistically large $r(0)$ values, >0.5, and was thus discarded. The fast component T_1 (hundreds of ps) is attributed to movements (partial rotation or wobbling) of the Re chromophore relative to the whole protein, which itself rotates much more slowly, with a ns rotation time T_2. The decrease of T_2 with decreasing concentration shows that all five Re-azurins are to some extent aggregated in solution. T_2 values then average over rotations of azurin complexes of various sizes and, possibly, also hindered rotations within loosely bound azurin aggregates. Partial dissociation of azurin aggregates is then manifested by a gradual decrease of T_2 instead of several decay components with concentration-dependent amplitudes. The movements of Re units become less restricted upon dissociation, as indicated by decreasing T_1 with dilution.

Relaxation Dynamics: Time-Resolved IR Absorption Spectra. Excitation of the $Re(CO)_3$(phen) chromophore in all five azurins and the free sensitizer **Re(im)** with 400 nm, ~150 fs laser pulses partially depletes the ground-state population.

(40) Braterman, P. S. *Metal Carbonyl Spectra*; Academic Press: London, 1975.
(41) Dattelbaum, D. M.; Omberg, K. M.; Schoonover, J. R.; Martin, R. L.; Meyer, T. J. *Inorg. Chem.* **2002**, *41*, 6071–6079.
(42) Dattelbaum, D. M.; Omberg, K. M.; Hay, P. J.; Gebhart, N. L.; Martin, R. L.; Schoonover, J. R.; Meyer, T. J. *J. Phys. Chem. A* **2004**, *108*, 3527–3536.
(43) Bredenbeck, J.; Helbing, J.; Hamm, P. *J. Am. Chem. Soc.* **2004**, *126*, 990.
(44) Lin, R.-J.; Lin, K.-S.; Chang, I.-J. *Inorg. Chim. Acta* **1996**, *242*, 179–183.

Table 2. Emission Decay Kinetics of Re-Azurins in Air-Equilibrated KP$_i$ (D_2O, pD ~7.1) Buffer (Emission Maxima E_m in nm, Lifetimes τ in ns)

	concentrated[b]					5× diluted				
	E_m	τ_1	τ_2	% A_1	% A_2	E_m	τ_1	τ_2	% A_1	% A_2
107-dmp	542	28 ± 0.8	129 ± 0.7	26	74	548	19 ± 0.6	153 ± 0.6	21	79
109-phen	550	19 ± 0.7	47 ± 0.9	43	57	556	9 ± 0.4	45 ± 0.2	20	80
124-phen	550	2 ± 0.1	42 ± 0.2	36	64	563	4 ± 0.1	50 ± 0.2	24	76
83-phen[a]	563	2 ± 0.1	43 ± 0.1	26	74	568	2 ± 0.1	47 ± 0.2	25	75
126-phen	572	19 ± 0.5	113 ± 0.4	22	78	–	17 ± 0.7	142 ± 0.5	16	84

	10× diluted					20× diluted				
	E_m	τ_1	τ_2	% A_1	% A_2	E_m	τ_1	τ_2	% A_1	% A_2
107-phen	553	14 ± 0.5	162 ± 0.5	19	81	553	15 ± 0.6	172 ± 0.6	19	82
109-phen	557	7 ± 0.3	46 ± 0.2	19	81	–	8 ± 0.4	48 ± 0.2	19	81
124-phen	565	3 ± 0.1	52 ± 0.2	23	77	568	3 ± 0.1	53 ± 0.2	28	72
83-phen[a]	574	2 ± 0.1	48 ± 0.2	26	74	–	2 ± 0.1	49 ± 0.2	27	73
126-phen	578	12 ± 0.4	147 ± 0.4	17	83	–	8 ± 0.3	143 ± 0.4	22	78

[a] Virtually identical decay kinetics were found for a concentrated solution of **83-phen** in KP$_i$ (H_2O, pH ~7.1): $\tau_1 = 2 \pm 0.1$ ns, $\tau_2 = 39 \pm 0.1$ ns, $A_1 = 24\%$, A_2: 76%. $E_m = 557$ nm. [b] Approximate initial concentrations (in mM): **83-phen**: 4.8, **107-dmp**: 5.0, **109-phen**: 6.0, **124**: 6.0,**126-phen**: 3.5.

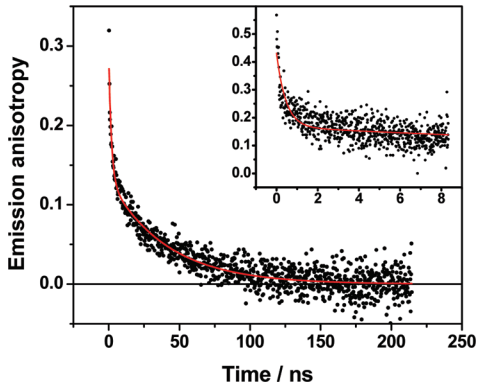

Figure 4. Emission anisotropy decay of **107-dmp** measured in KP$_i$ (D_2O, pD ~7.1) buffer. Data in the main graph were obtained with a time resolution of 228 ps/channel and used to determine T_2. Inset: 11.6 ps/channel, data used to determine T_1 while the T_2 value was fixed. Similar dependences were obtained for other Re-azurins (Table 3).

The conversion to an excited state in each case is accompanied by negative bleach and positive transient bands, respectively, which emerge in the TRIR spectra within the instrument time resolution (Figure 5 and Table 1). The excited-state ν(CO) IR spectral pattern of **Re(im)** and the Re-azurins is characteristic[12,14,18,32,41,42,45−47] of a Re → phen ^{3}MLCT excited state: all ν(CO) bands are shifted to higher energies relative to the ground state, and the separation between the A″ and A′(1) bands increases (Table 1); this IR assignment is supported by the **Re(Etim)** DFT-UKS calculation, which shows that the lowest excited state is attributable predominantly to a Re → phen ^{3}MLCT with smaller contributions from Etim → phen LLCT and phen-localized intraligand (IL) $\pi \rightarrow \pi^*$ (Figure 6). Two stable excited-state conformations were found by DFT for the Re^{I} complex in H_2O (Figure S4); the one with the im ligand pointing at phen (A) lies ~0.026 eV above conformation B where im points between the Re−CO and Re−N(phen) bonds (Figures 6 and S4). The calculated ν(CO) energies and their shifts upon excitation match well with experimental values (Table S6). (Optimized conformation structures, tables of frontier MOs, and allowed electronic transitions are summarized in the Supporting Information.)

Inspection of experimental TRIR spectra in the low-energy region (not shown) reveals that there are no features below the lowest A″ + A′(2) bleach band, excluding the possibility that a predominantly phen-based $\pi\pi^*$ ^{3}IL state is populated or that the Re(CO)$_3$(phen) unit is reduced.

TRIR spectra show a distinct temporal evolution, whereby the excited-state bands shift to higher energies over several hundreds of picoseconds. The shift is accompanied by much faster narrowing that is essentially completed during the first ~20 ps. These effects are most prominent for the two highest bands due to symmetric ν(CO) vibrations A′(1) and A′(2) (Figures 5 and 7). The dynamic IR spectral shift was analyzed quantitatively for the A′(1) band, which is well separated from the rest of the spectrum (Figure 7). To determine the A′(1) peak energies and bandwidths, the IR spectra of **107-dmp**, **109-phen**, **83-phen**, **126-phen**, and free **Re(im)** measured at selected time delays were fitted with a sum of Gaussian functions (Figure 8). (Gaussians gave better and more consistent results than Lorentzians used in our previous study[18] of **83-phen** and **109-phen**.) For **107-dmp**, strong overlap between the A′(1) band and the bleach decreases the accuracy of the fits at short time delays. The A′(1) band of **124-phen** is distinctly asymmetric, tailing toward lower energies. Although its shape can be fitted with two Gaussians, this type of fitting leads to results that are not consistent along the time evolution of the spectra, producing large discontinuities in bandwidths at several time delays. Instead, consistent fits were obtained (Figure 8) using an asymmetric log-norm function (eq 3)

$$y = h \times \exp(-0.693(\ln(1 + 2\gamma(x - p)/w)/\gamma)^2) \qquad (3)$$

where the individual symbols stand for the signal intensity (y), IR energy (x), maximum height (h) and energy (p) of the IR band maximum, width (w), and the asymmetry parameter (γ).

The time dependences of the A′(1) ν(CO) peak energies are shown in Figure 9. Experimental data $\tilde{\nu}(t)$ can be fitted either with a triexponential function (eq 4)

$$\tilde{\nu}(t) = \tilde{\nu}(\infty) - A_f \exp(-t/\tau_f) - A_i \exp(-t/\tau_i) - A_s \exp(-t/\tau_s) \qquad (4)$$

(45) George, M. W.; Johnson, F. P. A.; Westwell, J. R.; Hodges, P. M.; Turner, J. J. *J. Chem. Soc., Dalton Trans.* **1993**, 2977–2979.
(46) Dattelbaum, D. M.; Martin, R. L.; Schoonover, J. R.; Meyer, T. J. *J. Phys. Chem. A* **2004**, *108*, 3518–3526.
(47) Vlček, A., Jr.; Záliš, S. *Coord. Chem. Rev.* **2007**, *251*, 258–287.

Table 3. Time-Resolved Emission Anisotropy of Re-Azurins in Air-Equilibrated KP_i (D_2O, pD ~7.1) Buffer (Concentrations are Approximate)

	107-dmp		109-phen		83-phen		83-phen[a]
	5 mM	1 mM	6.0 mM	1.2 mM	4.8 mM	0.96 mM	6.0 mM
T_2/ns	40.8 ± 1.7	21.9 ± 1.5	17.5 ± 2	7.8 ± 1	7.4 ± 2.1	3.2 ± 0.7	5.1 ± 2.3
T_1/ps	454 ± 32	529 ± 43	239 ± 21[c]	144 ± 8[c]	398 ± 27	177 ± 9	343 ± 19

	126-phen					124	
	3.5 mM	1.4 mM	0.7 mM	0.35 mM	0.175 mM	6.0 mM	1.2 mM
T_2/ns	17.4 ± 1.5	11.0 ± 0.9	8.9 ± 0.8	7.4 ± 0.6	7.3 ± 0.7	26.5 ± 5.4	7.8 ± 1.7
T_1/ps	1370 ± 86	1045 ± 68	985 ± 62	294 ± 47[b]	561 ± 43	410 ± 23	284 ± 19

[a] Measured in KP_i (H_2O, pH ~7.1) buffer. [b] Poor fit. T_1 = 729 ± 153 ps, when determined from the long-range fit. [c] Fitting from 0 ps gives rather high $r(0)$ values. T_1 of 307 ± 31 and 162 ± 10 ps were obtained for 6.0 and 1.2 mM solutions, respectively, when fitting was begun at 23 ps.

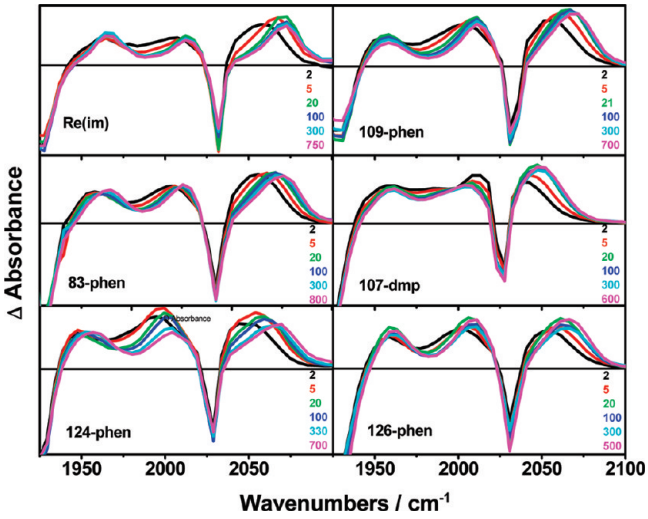

Figure 5. Difference time-resolved IR spectra of **Re(im)** and the Re-azurins in KP_i (D_2O, pD ~7.1) buffer measured at selected time delays after 400 nm, ~150 fs excitation. Experimental points are separated by 4.5−5.5 cm^{-1}. Sample concentrations are in the range 3.5−6 mM.

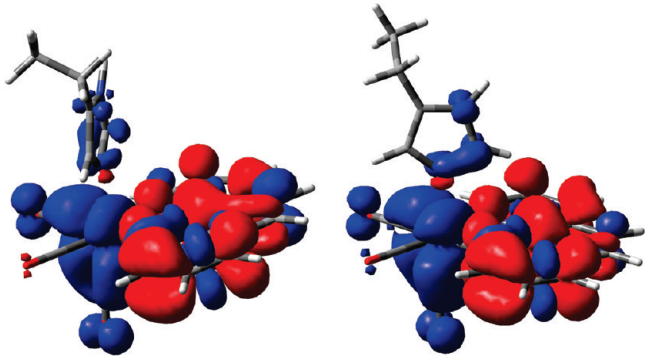

Figure 6. DFT-calculated (PBE0/CPCM-H_2O) electron density difference between the lowest ^{3}MLCT excited state and the ground state of **Re(Etim)** at the ^{3}MLCT optimized geometry in conformation B (left) and A (right). Blue and red show regions where the electron density decreases and increases upon excitation, respectively. MLCT character is indicated by the depopulated region around the Re atom, while the depopulated Etim ligand and phen regions reveal LLCT and $\pi\pi^*$ IL contributions, respectively.[47]

or a stretched exponential function (eq 5):

$$\tilde{\nu}(t) = \tilde{\nu}(\infty) - A_1 \exp(-t/\tau_1) - A_2 \exp(-t/\tau_2)^{\beta} \qquad (5)$$

Triexponential fitting (eq 4) yields three kinetics components, "fast", "intermediate", and "slow", τ_f, τ_i, and τ_s, respectively, the corresponding amplitudes A_f, A_i, and A_s, and the A′(1) ν(CO)

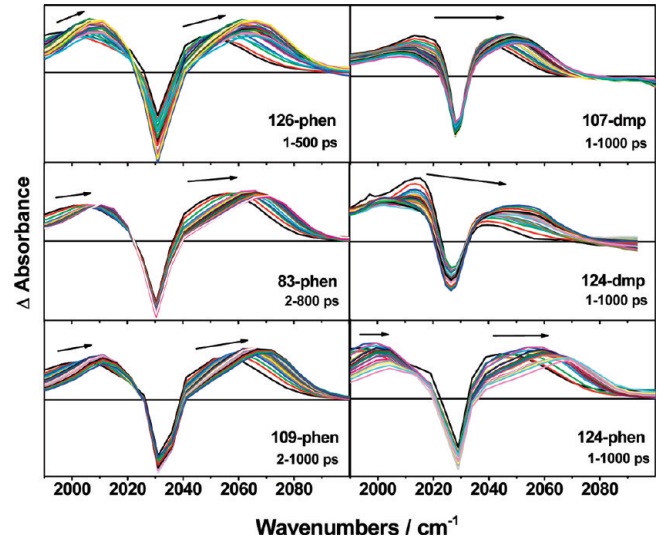

Figure 7. Difference TRIR spectra of the Re-azurins in the spectral region of the A′(1) ν(CO) band. Measured from 2 to 1000 ps after 400 nm, ~150 fs excitation, in KP_i (D_2O, pD ~7.1) buffer. The spectral bands shift with time toward higher wavenumbers. Experimental points are separated by 4.5−5.5 cm^{-1} for **126-phen**, **83-phen**, and **109-phen** and 2−3 cm^{-1} for **107-dmp**, **124-phen**, and **124-dmp**. Re-azurin concentrations are in the range 3.5−6 mM. A 4-point smoothing was applied to the **124-dmp** spectra.

energy in the relaxed excited state, $\tilde{\nu}(\infty)$. The total A′(1) bandshift upon excitation equals $\tilde{\nu}(\infty) - \tilde{\nu}$(GS) and the magnitude of the dynamic shift is estimated as the sum of the amplitudes $A_f + A_i + A_s$. The "instantaneous shift", which occurs within the instrument time resolution, is estimated as the difference between the total and dynamic shifts. The fitted curves and values of the kinetics parameters are given in Figure 9 and Table 4, respectively. The stretched-exponential fitting (eq 5 and Tables S7, S8) always combines the fast and intermediate components into the stretched function with a rather large spread (β = 0.4−0.6), and it singles out the slow component as a pure exponential. The τ_1 (eq 5) and τ_s (eq 4) values are similar. Further discussion will be based on results of the triexponential fitting (eq 4) that allows us to attribute physical meaning to each exponential term.[13]

The triexponential fitting works very well for **83-phen**, **109-phen**, **124-phen**, and **126-phen**. The IR dynamic shift of **107-dmp** is also triexponential, but the intermediate component is only poorly resolved because of a very small dynamic shift. Hence, a biexponential fit (*i.e.*, $A_i = 0$) is preferred. Moreover, the low accuracy of the A′(1) peak energies at short time delays propagates into the τ_f and A_f values and thus into the relative magnitudes of the instantaneous and dynamic shifts, especially

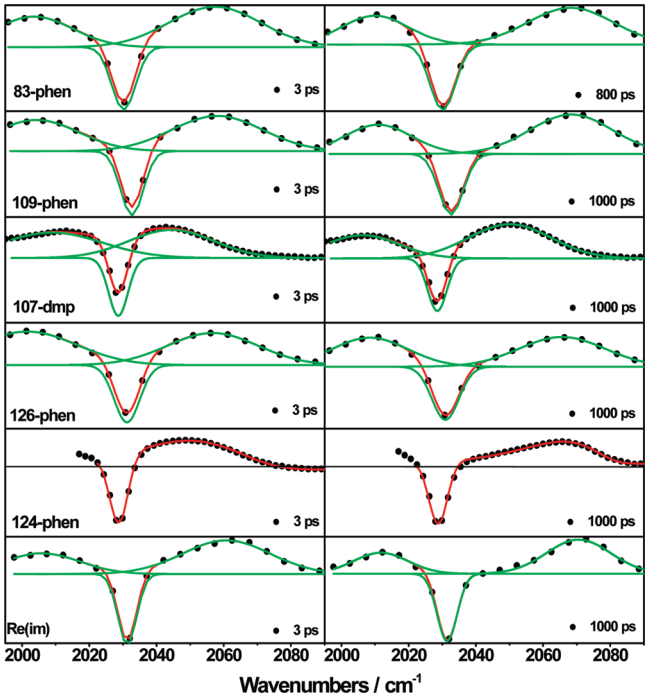

Figure 8. A′(1) band-shape fitting. Black: experimental points. Green: individual Gaussian bands. Red: final simulated spectrum. Spectra are fitted with three Gaussians corresponding to the A′(2) and A′(1) excited-state bands and the A′(1) bleach, except for spectra of **124-phen** that are fitted with eq 3, plus a Gaussian for the bleach. Sample concentrations are in the range 3.5−6 mM.

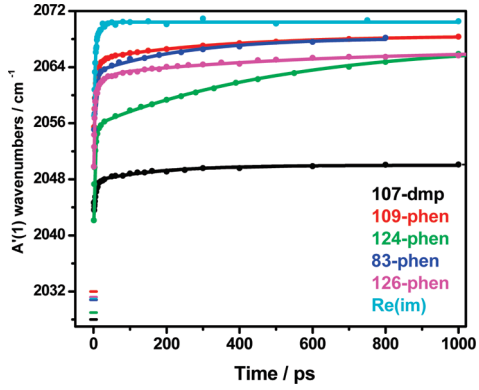

Figure 9. Time dependences of the peak energies of the A′(1) ν(CO) band of **83-phen** (blue), **107-dmp** (black), **109-phen** (red), **124-phen** (green), **126-phen** (magenta), and free **Re(im)** (cyan). The curves are the triexponential fits (eq 1) with parameters from Table 4 (concentrated samples).

in the case of the high-resolution experiment. The dynamic IR shift of free **Re(im)** does not show the slow component (A_s = 0) and was fitted biexponentially. The excited-state IR bands of Re-azurins are broader by ∼5 cm^{-1} than those of free **Re(im)**, and the A′(1) bandwidths decrease rapidly after *ca.* 10−20 ps.

Comparison of TRIR spectra of **124-phen** and **124-dmp** (Figure 7) indicates strong effects of phen methylation on the relaxation dynamics: the total shift is much smaller in **124-dmp**, ∼25 cm^{-1}, and the "instantaneous" shift is negative. Relaxation is manifested by a slow dynamic red shift that is still apparent between 3 and 3.7 ns. The very broad and asymmetric band shape, together with the strong overlap with the bleach, prevented reliable determination of relaxation parameters.

Concentration effects on the IR dynamics of **107-dmp**, **124-phen**, and **126-phen** are summarized in Table 5 and Figures S5−7. The fast and intermediate kinetics components are essentially independent of concentration. The time constant of the "slow" kinetics component of **107-dmp** increases upon dilution, reaching a value comparable to that measured for **83-phen**. Its amplitude and, hence, the total shift also slightly increase. The dynamic behavior of **124-phen** and the shape of the A′(1) asymmetric band are independent of concentration. **126-phen** shows a systematic decrease of τ_s upon dilution.

Discussion

The TRIR experiments show that electronic excitation of Re(CO)$_3$(phen) covalently attached to azurin triggers a multitude of dynamic relaxation processes whose rates span a broad time range, depending on protein surface locations. Structural and time-resolved emission data point to association between azurin molecules in crystals as well as solutions. We will attempt to interpret relevant relaxation processes and molecular motions in terms of the available structural data and solution behavior. We assume that the principal structural features of metallolabel sites and their aggregated forms in crystals are preserved in solutions.

The key observations are as follows: crystal structures reveal that the environment around the Re chromophore and interactions between azurin molecules are strongly dependent on the metallolabel site location; depending on this location, some of the CO ligands interact with the peptide chains by H-bonds, dipole−dipole interactions, and/or van der Waals forces and part of the Re chromophore is exposed to the solvent and the phen ligands either face the peptide on one side and the solvent on the other (**83-phen**, **109-phen**, **126-phen**) or form hooked dimers through $\pi\pi$ stacking of two Re units (**107-dmp** and **124-phen**). Re-Azurins weakly associate in ∼mM solutions with the tendency to form aggregates increasing in the order **83-phen** < **109-phen** < **126-phen** ≈ **124-phen** ≪ **107-dmp**, as judged by the ns kinetics component (T_2) of the emission anisotropy decay. Azurin solutions contain monomers and dimers (or trimers for **107-dmp**), probably together with weakly bound aggregates. TRIR spectra together with DFT calculations confirm that the lowest excited state of **Re(Etim)** as well as each of the five Re-azurins is predominantly ^{3}MLCT (charge transfer from Re^{I}(CO)$_3$(im) to phen); the azurin Cu^{II} center partially quenches the ^{3}MLCT emission by both intra- and intermolecular (*i.e.*, within the Re-azurin aggregates) energy transfer, giving rise to multiexponential decays; and the relaxation dynamics are manifested by shifts of excited-state IR bands to higher energies that occur without substantial change of the overall spectral pattern. Relaxation can be analyzed in terms of triexponential kinetics (the magnitude of the overall spectral shift and the three lifetimes with their associated amplitudes being the most relevant kinetics parameters). The "slow" relaxation lifetime τ_s is the most structure-sensitive parameter reporting on the metallolabel binding site dynamics; the presence of the ∼10^2 ps T_1 component of the emission anisotropy decay shows that the Re chromophore undergoes hindered rotation or a wobbling motion relative to the protein backbone. Although their time scales are similar, there is no general quantitative correspondence between rotation T_1 and relaxation τ_s times, and notably, their Re location and sample-concentration dependences are different.

Table 4. Dynamic Shift Parameters of the A′(1) ν(CO) Band of Re-Azurins and **Re(im)** in KP_i (D_2O, pD ~7.1) Buffer at 21 °C[a]

	109-phen[b]	83-phen[b]	124-phen	126-phen	107-dmp, LR	107-dmp, HR	Re(im)
ν_{GS}, cm^{-1}	2032.6	2030.2	2028.9	2030.8	2027.6	2028	2031.4
$\nu(\infty)$, cm^{-1}	2068.5	2068.4	2067.4	2066.4	2053.6	2050	2070.4
total shift	36	38	38.5	35.6	26	22	39
inst. shift	14.8	16.8	9.4	6.1	6.4	14	12
dyn. Shift	21.2	21.4	29.0	29.5	19.5	8.0	27
A_s, cm^{-1}	3.4 ± 0.1	5.0 ± 0.2	11.7 ± 0.1	3.7 ± 0.2	2.8 ± 0.9	2.3 ± 0.1	–
A_i, cm^{-1}	3.0 ± 0.3	6.2 ± 2.9	5.2 ± 1.8	3.7 ± 0.5	1.4 ± 0.8	–	4.5 ± 1.1
A_f, cm^{-1}	14.8 ± 0.3	10.2 ± 1.9	12.2 ± 1.3	22.1 ± 3.3	15.3 ± 1.0	5.7 ± 0.2	22.4 ± 1.3
τ_s, ps	358 ± 25	287 ± 34	539 ± 12	570 ± 79	176 ± 78	181 ± 20	–
τ_i, ps	14.0 ± 1.5	7.0 ± 2.1	7.8 ± 1.8	18.5 ± 4.5	25 ± 33	–	12.8 ± 2.9
τ_f, ps	2.7 ± 0.1	1.9 ± 0.8	2.0 ± 0.5	1.5 ± 0.2	2.6 ± 0.4	5.7 ± 0.4	2.3 ± 0.3

[a] Re-azurin concentrations are in the range 3.5−6 mM. Parameters are based on Gaussian band-shape fitting of **Re(im)**, **83-phen**, **109-phen**, **107-dmp**, **126-phen**, and asymmetric log-norm fitting of **124-phen**. Two sets of results are presented for **107-dmp**: a triexponential fit of spectra obtained with 4.5−5.5 cm^{-1} resolution (LR) and a biexponential fit of spectra obtained with 2−3 cm^{-1} resolution (HR). Kinetics fitting was begun at 2 ps. [b] Based on TRIR spectra[18] that were refitted with Gaussian functions and triexponential kinetics; the kinetics data presented herein are somewhat different from those reported earlier[18] employing Lorentzian fitting and biexponential kinetics.

Table 5. Dynamic Shift Parameters of the A′(1) ν(CO) Bands of **107-dmp**, **124**, and **126-phen** in KP_i (D_2O, pD ~7.1) Buffer Measured as a Function of the Azurin Concentration at 21 °C[a]

	107-dmp			124-phen			126-phen		
	5.7 mM	1.9 mM	0.48 mM	4.3 mm	1.07 mM	0.54 mM	4.0 mM	0.8 mM	0.4 mM
ν_{GS}, cm^{-1}	2028	2028	2028	2028.9	2028.9	2028.9	2030.8	2030.8	2030.3
$\nu(\infty)$, cm^{-1}	2050.0	2050.5	2051.5	2067.4	2067.2	2067.4	2066.4	2065.3	2062.6
total shift	22.0	22.5	23.5	38.5	38.3	38.5	35.6	34.6	32.3
inst. shift	14	14.6	14.7	9.4	11.6	13.7	6.1	2.3	6.7
dyn. Shift	8.0	7.9	8.8	29.1	26.7	24.8	29.5	32.3	25.6
A_s, cm^{-1}	2.3 ± 0.1	2.2 ± 0.1	2.4 ± 0.2	11.7 ± 0.1	10.8 ± 0.1	10.9 ± 0.2	3.7 ± 0.2	3.3 ± 0.2	2.6 ± 0.5
A_i, cm^{-1}	–	–	–	5.2 ± 0.5	2.9 ± 1.6	1.6 ± 0.9	3.7 ± 0.5	4.1 ± 1.1	2.9 ± 1.2
A_f, cm^{-1}	5.7 ± 0.2	5.7 ± 0.4	6.4 ± 0.5	12.2 ± 1.3	13.0 ± 1.1	12.3 ± 0.9	22.1 ± 3.3	24.9 ± 4.9	20.1 ± 3.8
τ_s, ps	181 ± 20	205 ± 31	296 ± 54	539 ± 12	500 ± 16	555 ± 29	570 ± 79	416 ± 70	280 ± 96
τ_i, ps	–	–	–	7.8 ± 1.8	12.0 ± 5.4	25.6 ± 21	18.5 ± 4.5	12.1 ± 4.2	16.3 ± 11.3
τ_f, ps	5.7 ± 0.4	5.7 ± 0.4	5.6 ± 0.5	2.0 ± 0.4	2.7 ± 0.5	3.1 ± 0.5	1.5 ± 0.2	1.5 ± 0.3	1.8 ± 0.5

[a] Parameters are based on Gaussian band-shape fitting of high-resolution TRIR spectra of **107-dmp** and asymmetric log-norm fitting (eq 3) of high-resolution TRIR spectra of **124-phen**. Kinetics fitting was begun at 2 ps.

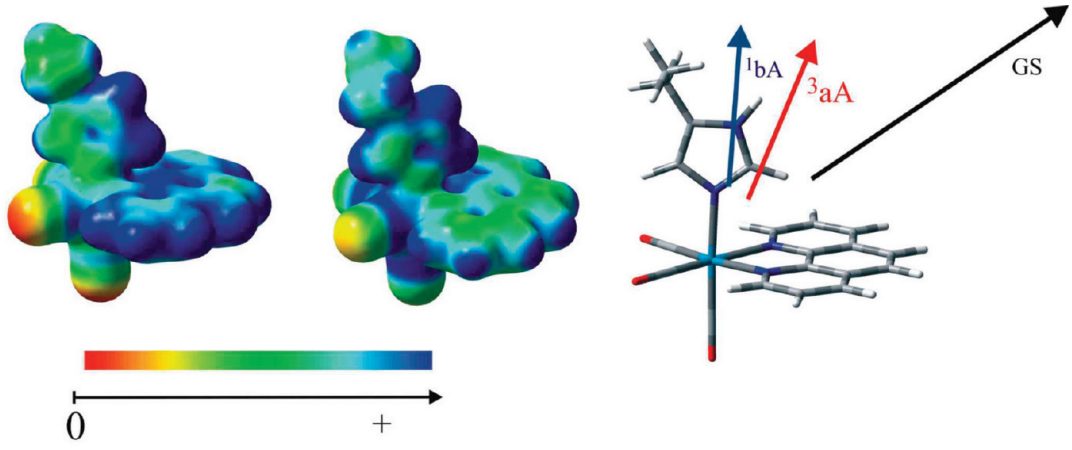

Figure 10. Mapping of the electrostatic potential onto an isodensity surface of the ground state (left) and the relaxed lowest ^{3}MLCT state a^3A (center) of **Re(Etim)**. Right: The relative size and orientation of dipole moment vectors of the ground state (black), the optically populated ^{1}MLCT state b^1A (blue), and the relaxed ^{3}MLCT state a^3A (red) of **Re(Etim)** projected onto an optimized ground-state molecular structure (DFT PBE0/CPCM calculation in H_2O; b^1A and a^3A obtained by TDDFT and UKS, respectively: the dipole moment vectors originate in the center of charge; the coordinate system is identical for b^1A and a^3A).

Relaxation Processes Triggered by Excitation. Population of the Re-label ^{3}MLCT state occurs in ~130 fs[48] after excitation, redistributing ≥6000 cm^{-1} of energy and changing the charge distribution (Figure 10). Ensuing relaxation includes intramolecular vibrational energy redistribution (IVR) into low-frequency, large-amplitude skeletal modes; vibrational energy relaxation (cooling) by energy dissipation into the immediate chromophore environment; and heat dissipation into the bulk solvent and/or the protein. The medium, which consists of water (D_2O) molecules and nearby amino acid residues, responds to the perturbed charge distribution by femtosecond electronic polarization, inertial solvent movements, and much slower (ps) molecular reorientation.

(48) Cannizzo, A.; Blanco-Rodríguez, A. M.; Nahhas, A.; Šebera, J.; Záliš, S.; Vlček, A., Jr.; Chergui, M. *J. Am. Chem. Soc.* **2008**, *130*, 8967–8974.

The subps "instantaneous" IR shift reports on the fastest of these processes, *viz*. the change of charge distribution upon excitation and intersystem crossing, IVR, electronic polarization of the medium as well as inertial, and part of the reorientational relaxation of the D_2O solvent. Whereas $\sim 10^1-10^2$ fs water relaxation (possibly together with some ultrafast protein motions) has been identified[49−51] as a substantial contributor to the protein dynamics, it cannot be separated from other photophysical processes by TRIR spectroscopy of the ^{3}MLCT state. Nor can the hypothetical spectrum at $t = 0$ be determined, preventing us from estimating the amount of ultrafast solvent relaxation.

The "fast" relaxation kinetics (τ_f) component observed for Re-azurins is independent of the location of the metallolabel binding site; and the values reported herein are comparable to those determined for various Re carbonyl-diimine complexes in dipolar solvents[12,14−16,52,53] including **Re(im)** in D_2O (Table 4) and in ionic liquids.[13] Accordingly, this component can be attributed to the later stages of IVR, which include equilibration between low-frequency modes of the chromophore as well as closely interacting solvent (D_2O) molecules (local solvent).[14]

The "intermediate" kinetics component is virtually azurin-independent, so far as its limited accuracy allows us to judge, and it has a low amplitude. The "intermediate" IR shift is comparable to the "slow" relaxation component of the biexponential relaxation dynamics observed in dipolar solvents,[12,14−16,52,53] including **Re(im)** in D_2O (Table 4). A similar "intermediate" component was observed in ionic liquids, but with longer lifetimes, 40−80 ps.[13] This component is attributed to vibrational cooling that involves also restructuring of the local solvent[14] and heat dissipation into the medium. The latter process contributes very little (if at all), since the expected[54] correlation of the relaxation rates τ_i^{-1} with medium thermal diffusivity was found in neither dipolar solvents[53] nor ionic liquids.[13]

The "slow" kinetics component of the dynamic IR shift is protein-specific, reporting on the dynamics of the Re binding site. In particular, τ_s measures the rate of medium response to the sudden charge redistribution in the Re chromophore upon excitation.[13] Polar residues on the peptide chains and associated water molecules exert an anisotropic electric field on the Re chromophore (the "reaction field"). At the instant of excitation, the reaction field is oriented to match the ground-state charge distribution in the Re chromophore. Since the ^{3}MLCT state is less polar than the ground state (Figure 10),[13,55] the reaction field is initially directed opposite to the charge redistribution driven by excitation. Relaxation of the Re binding site after excitation weakens and reorients the reaction field, allowing the charge distribution in the metallolabel to develop to the extent described by the ^{3}MLCT wave function (Figure 6). The "slow" IR spectral shift closely monitors the relaxation process, owing to ν(CO) sensitivity to the electron density distribution and anharmonic coupling, which also depends[15] on the reaction field. This shift thus reports on those molecular motions that change electrostatic or hydrogen-bonding interactions between the chromophore and its medium. Displacement or reorientation of the $Re(CO)_3$(phen) unit relative to the peptide chain is the most likely mechanism of the "slow" relaxation process. The TRIR experiment alone cannot distinguish the effects of torsional motions of solvated peptide chains in the vicinity of the Re binding site from bending or rotating the $Re(CO)_3$(phen) moiety relative to the protein that may occur around the His $C^{\alpha}-C^{\beta}$ bond connecting the im ligand to the peptide or around the Re−N(im) bond. The presence of an $\sim 10^2$ ps T_1 component of the emission anisotropy decay kinetics provides evidence that the Re chromophore undergoes hindered rotation or wobbling that changes its orientation relative to that at the instant of excitation. Such motions would affect the IR dynamics shift only if they change the orientation of the $Re(CO)_3$(phen) unit relative to nearby charged or polar peptide side chains, thereby perturbing the reaction field. The T_1 process also can involve motions of the peptide arm that bears the Re chromophore, leaving the immediate metallolabel binding environment and, thus, the reaction field, intact. Comparison of T_1 and τ_s values reveals important quantitative differences between the dynamics manifested in TRIR and emission anisotropy: T_1 is longer than τ_s for **83-phen**, **107-dmp**, and **126-phen** but slightly shorter for **124-phen** and **109-phen**. T_1 and τ_s also depend on the Re location in different ways: τ_s increases in the order **107-dmp** < **83-phen** < **109-phen** < **124-phen** ≤ **126-phen**, while T_1 follows the order **109-phen** < **83-phen** < **107-dmp** ≈ **124-phen** ≪ **126-phen**. It follows that only some of the reorientational motions reported by the T_1 anisotropy decay contribute to the relaxation processes that give rise to the IR dynamic shifts. It is likely that the T_1 anisotropy decays of **83-phen**, **107-dmp**, and **126-phen** mostly originate in segmental motions of Re-bearing β-strands relative to the rest of the molecule, as observed for other proteins.[56] On the other hand, reorientation and relaxation movements appear to coincide for **109-phen**.

Metallolabel Site Dynamics in Re-Azurins. The strong dependence of the "slow" IR relaxation component τ_s (Figure 8, Table 4 and 5) and the fast rotation time T_1 (Table 3) on the Re location shows that each of the five Re-azurins has a unique dynamics, requiring us to discuss them case by case:

83-phen has the least tendency to associate in solution, and neither $\pi\pi$ stacking nor specific interactions between the peptide and CO ligands were observed in the crystal.[11,18] The ground-state IR spectrum indicates that the CO ligands are essentially equivalent. Relaxation is relatively fast, $\tau_s \approx 290$ ps, and the associated movements likely involve displacements of negatively charged peptide side chains away from the phen ligand that becomes negatively charged upon excitation. The T_1 rotation time is slower than relaxation but drops with concentration. It probably corresponds to the wobbling of the Re-bearing β-strand, whose motion is restricted at higher concentrations by azurin association.

The behavior of **109-phen** is similar to that of **83-phen**, although it associates in solution to a greater extent and its crystal structure consists of two distinct units, each containing two conformations with different orientations of the Re

(49) Jordanides, X. J.; Lang, M. J.; Song, X.; Fleming, G. R. *J. Phys. Chem. B* **1999**, *103*, 7995–8005.
(50) Halder, M.; Mukherjee, P.; Bose, S.; Hargrove, M. S.; Song, X.; Petrich, J. W. *J. Chem. Phys.* **2007**, *127*, 055101/1−055101/6.
(51) Nilsson, L.; Halle, B. *Proc. Natl. Acad. Sci. U.S.A.* **2005**, *102*, 13867–13872.
(52) Busby, M.; Gabrielsson, A.; Matousek, P.; Towrie, M.; Di Bilio, A. J.; Gray, H. B.; Vlček, A., Jr. *Inorg. Chem.* **2004**, *43*, 4994–5002.
(53) Blanco-Rodríguez, A. M.; Towrie, M.; Ronayne, K. L.; Záliš, S.; Vlček, A., Jr. Manuscript in preparation.
(54) Iwata, K.; Hamaguchi, H. *J. Phys. Chem. A* **1997**, *101*, 632–637.
(55) Walters, K. A.; Kim, Y.-J.; Hupp, J. T. *Inorg. Chem.* **2002**, *41*, 2909–2919.
(56) Lakowicz, J. R. *Principles of Fluorescence Spectroscopy*, 3rd ed.; Springer: New York, 2006.

complex relative to the protein and different H-bonding with the His109 imidazole (Figure 2).[18] Relaxation movements are again attributed to displacement of the peptide groups of both the main and side chains[18] away from phen, to weaken unfavorable charge−charge interactions. These motions likely involve rotation of the His109 imidazole group relative to the peptide chain and of $Re(CO)_3$(phen) relative to the imidazole, in addition to peptide torsions. Structural flexibility around the His $C^{\alpha}-C^{\beta}$ and Re−N(im) bonds is documented by the presence of two conformations in the crystal structure. The same motions contribute to the T_1 rotation time that is shorter than the relaxation time τ_s; they accelerate upon dissociation of azurin aggregates at lower concentration. Relaxation movements in **109-phen** are slower than those in **83-phen**, possibly due to some hindrance caused by H-bonding between the peptide and the im and one of the equatorial CO ligands or lower flexibility of the Re-bearing β-strand.

126 forms dimers where each phen is in a van der Waals contact with side chains from its own molecule below and the adjacent molecule above. The T_2 slow rotation time decreases significantly with dilution but shows that **126** is still partially dimerized even at 0.35 mM. The relaxation motions (τ_s) are rather slow, ~570 ps at 4.0 mM Re-azurin, but accelerate to ~420 and ~280 ps upon 5- and 10-fold dilution, respectively. Relaxation in the dimer probably involves relative motion of the peptide chains of the two molecules and the Re label to minimize the peptide−phen and peptide−CO Coulombic interactions. Such motions are rather slow because they occur at a protein−protein interface. They could be hindered by the axial CO interacting with the other molecule and one equatorial CO interacting with the C-terminal carboxylate 4 Å apart, as indeed is reflected by slow τ_s values at high concentrations. The phen ligands probably interact only weakly with Gln107 of one molecule, Met109 from the other, and Glu104 of the same molecule, but 5.0 Å away. Hence only little displacement is required. Relaxation becomes much faster upon dimer dissociation, as it is now determined mainly by interactions between the Re chromophore and peptide chain of only one side of phen, while the other is solvated. These interactions are weaker than those in the dimer, and the amplitude A_s drops upon 10-fold dilution of 4.0 mM protein from 3.7 cm^{-1} to 2.6 cm^{-1}. The T_1 anisotropy decay is the slowest observed in this study, ~1 ns, and occurs with the lowest amplitude. It accelerates slightly with decreasing concentration, while the amplitude diminishes further. The observation that T_1 is much larger than τ_s at all investigated concentrations indicates that most of the motions responsible for the T_1 anisotropy decay are different from the relaxation motions manifested in the IR dynamic shift. The T_1 anisotropy decay can be attributed to slow segmental movements of the Re-bearing β strand. It is slower in the dimer because of interactions between the two parallel β strands.

The phen ligand of the Re label in **124-phen** is in an asymmetric environment, being solvated on one side and interacting with a phen ligand from the second molecule through $\pi\pi$ stacking. One of the equatorial CO ligands is directed against the peptide chain of the same molecule, although the distance to the nearest charged group is 4−5 Å. Anisotropy decay T_2 shows that the dimers largely persist in ~6 mM solution, where the ground-state IR spectrum reveals nonequivalence among the three CO ligands. Relaxation is relatively slow ($\tau_s \cong 530$ ps), and the corresponding amplitude A_s is the largest among the five Re-azurins. Both the rate and amplitude are concentration-independent, indicating that relaxation is dominated by structural and/or solvation changes on the side of the phen ligand that is exposed to solvent and/or by movements of peptide groups interacting with equatorial CO ligands (Figure 2). The highly asymmetric shape of the excited-state IR band (Figures 5, 7, and 8) points to complicated relaxation dynamics and/or the presence of several excited-state conformers. We cannot exclude the possibility that the crystal structure (Figure 2) in this case does not describe the solution aggregates properly. The instantaneous shift systematically increases upon dilution, indicating an increasing contribution from ultrafast solvation. The anisotropy decay T_1 is faster than relaxation but exhibits a different concentration dependence, decreasing upon dilution. Re-Label rotation thus could be a contributor to the relaxation process, although not the predominant one.

Comparison of **124-phen** and **124-dmp** TRIR spectra (Figure 7) reveals a large effect of phen methylation; the spectra of **124-dmp** indicate a negative instantaneous shift followed by a very slow, low-amplitude shift to higher energies. The overall shift of **124-dmp** is much smaller than that of **124-phen** (24 vs 38.5 cm^{-1}), a difference that is tentatively attributed to greater mixing between MLCT and $\pi\pi^*$ IL wave functions in the lowest **124-dmp** excited state; such mixing also was proposed in a low-temperature emission study of $[Re(Cl)(CO)_3(N,N)]$.[57] It follows that the extent of charge transfer from $Re^{I}(CO)_3$(im) to dmp upon excitation is much smaller than that for phen. Excitation-triggered fluctuations in **124-dmp** are slowed by friction and steric hindrance attributable to the methyl groups.

The total shift (22−26 cm^{-1}) of **107-dmp** is comparable to that of **124-dmp** and much smaller than that for phen-containing Re-azurins, but unlike **124-dmp**, the instantaneous shift is positive, demonstrating that the electronic structure is affected by the environment from the earliest times after excitation. The **107-dmp** crystal structure contains a dimer of $Re(CO)_3$(dmp) units "hooked" by $\pi\pi$-stacking that is capped by a third azurin molecule. The Re center is sequestered and largely shielded by peptide chains, and the CO ligands lie in tight pockets. Very large T_2 values show that trimers are present in solution, only partially dissociating upon dilution. The IR dynamical shift, which is faster ($\tau_s \cong$ 180 ps) than in other Re-azurins, has a very small amplitude. We propose that the tight Re binding site in **107-dmp** and the bulkiness of the dmp ligand disfavor many of the fluctuations observed for other Re-azurins. Only spatially limited, fast initial relaxation motions are possible. Upon trimer or dimer dissociation, the metallolabel becomes more exposed, and additional fluctuations can occur on a slower time scale. Accordingly, the τ_s relaxation time increases with decreasing concentration, and T_1 is substantially larger than τ_s, which is attributed to tumbling of the entire metallolabel site.

Concluding Remarks. Solvation dynamics in protein environments are commonly investigated by measuring dynamic fluorescence Stokes shifts (FSSs) of suitable fluorescent probes that are bound to the protein either covalently (*e.g.*, tryptophan indole or *N*,*N*-diamino-napthyl side group of aladan, an un-

(57) Striplin, D. R.; Crosby, G. A. *Coord. Chem. Rev.* **2001**, *211*, 163–175.

natural amino acid) or noncovalently (*e.g.*, coumarin-153 or eosin).[49−51,58−66] The probes are assumed not to be polarizable, so that variations in the energy gap between the fluorescent and ground electronic states can be attributed to changes in solvation energy in a changing reaction field and, through the linear response approximation, linked to spontaneous fluctuations of the electrostatic field of the solvated protein.[49−51,58,65] Such reaction-field fluctuations can in principle be predicted from frequency-dependent dielectric dispersion,[49,50] if known. Generally, FSS studies have identified important subpicosecond contributions from water dynamics,[49,50,58] whereas solvated protein motions dominate on tens-to-hundreds-ps time scales.[49,51,58] For covalently attached fluorescent probes, fluorophore self-motions cannot be distinguished from peptide movements and could make important contributions.[51] The effect of probe location on dynamic FSSs has been investigated for a globular protein:[58] whereas a Trp-location-independent 80−140 fs kinetics component due to solvent is present, the rate of the slower dynamics varies: relaxation times of ∼100 ps, 100−1000 ps, and ∼10 ns were reported for solvent-exposed, partially exposed, and buried sites, respectively.[58] A similar study of apomyoglobin revealed 1−8 and 20−200 ps kinetics components of Trp FSSs, the latter attributed to "collective water network rearrangements coupled with protein fluctuations".[66] Although there have been extensive experimental and computational investigations, as yet there is no unified model relating motions in solvated protein environments to dynamic FSSs, with the interpretation of ultrafast water reorganization and the roles of protein and bound-water motions in slower protein solvation dynamics being the most controversial issues.[65] It is possible that formulation of a general mechanism is beyond reach, as the observed dynamics could involve a multitude of (coupled) motions whose character and relative weight depend not only on the protein but also on the type of probe and its location. (Note that a subps FSS was not reported for Trp in apomyoglobin,[65,66] whereas <300 fs kinetics account for 60% of coumarin-153 FSS.[50]) Our TRIR approach featuring a ^{3}MLCT-excited organometallic probe is complementary to FSSs. Although subps information is inevitably lost because of convoluted photophysics, IVR, and vibrational relaxation, our method provides new insights into the $\sim 10^2$ ps dynamics. Shifts of ν(CO) report on the effects of changing the reaction field on intramolecular vibrations (*i.e.*, coupling of motions along outer-sphere and internal coordinates). It is likely that specific electrostatic interactions of the phen and/or CO ligands with charged or polar peptide side groups play a more important role than the overall reaction field at the chromophore, while changes in H-bonding can contribute as well. Vibrational normal coordinates also can be affected by structural changes in the peptide during relaxation, and such effects can extend over long molecular distances.[67] The electronically excited Re complex is highly polarizable; the IR response to medium relaxation involves changes in charge distribution in the excited-state wave function. The "slow" ν(CO) shift kinetics are interpreted in terms of the same kinds of motions that are responsible for FSSs. However, the Re-azurin relaxation measured by TRIR is somewhat slower than most of the FSS solvation times reported previously for other proteins. In the absence of a detailed understanding of the underlying motions and their coupling to Re-label vibrations, we cannot make a strong link between observed ν(CO) shifts and spontaneous fluctuations of the protein environment, since the linear response approximation may not hold.[17] Unlike most fluorescent probes, the Re chromophore is a low-symmetry three-dimensional molecule, possibly prone to local solvation by organized solvent molecules that can undergo restructuring during relaxation.[14,17,53,68] In any case, it is clear that ^{3}MLCT excitation triggers extensive dynamical structural changes in the Re binding site and its surroundings, which through feedback affect the excited label itself. The same changes will occur in proteins where Re-label excitation also induces long-range ET, and most importantly, the two processes likely will be coupled.

We conclude that time-resolved IR spectroscopy and emission anisotropy of Re^{I} carbonyl-diimine complexes are powerful probes of dynamical responses of molecular units at or around protein surfaces and protein−protein interfacial regions. Labeling of azurin surface histidines with $Re(CO)_3$(phen) does not perturb the peptide fold but enhances aggregation by label−peptide interactions (**126-phen**, **83-phen**, **109-phen**), label−label (*i.e.*, phen−phen) $\pi\pi$ stacking (**124-phen**), or both (**107-dmp**). The lowest triplet excited state of Re(im)$(CO)_3$(phen) is predominantly $Re(CO)_3$ → phen MLCT with a contribution from im → phen LLCT. Optical excitation of the Re label triggers a multitude of relaxation processes that span time ranges from femtoseconds up to the first few nanoseconds. The "slow" ($\sim 10^2$ ps) kinetics component of the ν(CO) dynamic shift is Re-site specific. It is attributed to a multitude of peptide and label torsional motions whereby the excited $Re^{I}(CO)_3$(phen)(im) unit is displaced to optimize chromophore−peptide dipole−dipole and H-bonding interactions. H-Bonds between the N^{δ} atom of the imidazole ligand and the peptide could play a role for **83-phen** and **109-phen**. Label self-motion (rotation around Re−N(im) or im-peptide bonds) seems to be involved for **109-phen** and, perhaps, **124-phen**. Such self-motions are not likely to contribute to the ν(CO) shifts of **126-phen** and **107-dmp**, which undergo segmental movements of Re-bearing β-strands or tumbling motions that change the orientation of the metallolabel without perturbing the reaction field or interactions with the peptide. Our work shows clearly that ps and ns protein dynamics must be taken into account in interpretations of the early events of phototriggered ET reactions of Re-azurins.

Acknowledgment. This work was supported by EPSRC (EP/E060544), STFC (CMSD43), COST D35, Ministry of Education of the Czech Republic (OC09043 and LC06063), NSF (CHE-0802907 and CHE-0749997), and NIH (DK019038).

Supporting Information Available: Tables of experimentally determined orientation of the histidine imidazole ligand relative

(58) Abbyad, P.; Shi, X.; Childs, W.; McAnaney, T. B.; Cohen, B. E.; Boxer, S. G. *J. Phys. Chem. B* **2007**, *111*, 8269–8276.
(59) Zhong, D.; Pal, S. K.; Wan, C.; Zewail, A. H. *Proc. Natl. Acad. Sci. U.S.A.* **2001**, *98*, 11873–11878.
(60) Amisha Kamal, J. K.; Zhao, L.; Zewail, A. H. *Proc. Natl. Acad. Sci. U.S.A.* **2004**, *101*, 13411–13416.
(61) Qiu, W.; Kao, Y.-T.; Zhang, L.; Yang, Y.; Wang, L.; Stites, W. E.; Zhong, D.; Zewail, A. H. *Proc. Natl. Acad. Sci. U.S.A.* **2006**, *103*, 13979–13984.
(62) Bhattacharyya, S. K.; Wang, Z.-G.; Zewail, A. H. *J. Phys. Chem. B* **2003**, *107*, 13218–13228.
(63) Pal, S. K.; Zewail, A. H. *Chem. Rev.* **2004**, *104*, 2099–2123.
(64) Pal, S. K.; Peon, J.; Zewail, A. H. *Proc. Natl. Acad. Sci. U.S.A.* **2002**, *99*, 1763–1768.
(65) Li, T.; Hassanali, A. A.; Kao, Y.-T.; Zhong, D.; Singer, S. J. *J. Am. Chem. Soc.* **2007**, *129*, 3376–3382.
(66) Zhang, L.; Wang, L.; Kao, Y.-T.; Qiu, W.; Yang, Y.; Okobiah, O.; Zhong, D. *Proc. Natl. Acad. Sci. U.S.A.* **2007**, *104*, 18461–18466.
(67) Fraga, E.; Loppnow, G. R. *J. Phys. Chem. B* **1998**, *102*, 7659–7665.
(68) Moret, M.-E.; Tavernelli, I.; Rothlisberger, U. *J. Phys. Chem. B* **2009**, *113*, 7737–7744.

to the $Re(CO)_3(phen)$ unit in the five proteins, DFT-calculated frontier Kohn−Sham orbitals and electronic transitions of **Re(Etim)** in two conformations, comparison of calculated and experimental ground- and excited-state ν(CO) IR wavenumbers of **Re(Etim)**, and results of stretched-exponential fitting of the A′(1) ν(CO) band shift kinetics at different concentrations. Figures of DFT-calculated structures of **Re(Etim)** in several ground- and excited-state conformations and time traces of the peak energy of the A′(1) ν(CO) band of **107-dmp**, **124-phen**, and **126-phen** measured at different concentrations. Full text of ref 33 (Gaussian 03 software) is provided. This material is available free of charge via the Internet at http://pubs.acs.org.

JA902744S